Volume 1 | Number 1 | Jan 2013 | Pages 1–100

Journal of
Materials Chemistry A

Materials for energy and sustainability
www.rsc.org/materialsA

Li⁺

ROYAL SOCIETY
OF CHEMISTRY

ROYAL SOCIETY
OF CHEMISTRY

www.rsc.org/materialsA

ARTICLE

Investigation into the effect of Fe-site substitution on the performance of $Sr_2Fe_{1.5}Mo_{0.5}O_{6-\delta}$ anodes for SOFCs

Jie Feng,[a] Guoquan Yang,[a] Ningning Dai,[a] Zhenhua Wang,[a] Wang Sun,[a] David Rooney,[b] Jinshuo Qiao*[a] and Kening Sun*[a]

Ni-substituted $Sr_2Fe_{1.5-x}Ni_xMo_{0.5}O_{6-\delta}$ (SFNM) materials have been investigated as anode catalysts for intermediate temperature solid oxide fuel cells. Reduced samples (x = 0.05 and 0.1) maintained the initial perovskite structure after reduction in H_2, while metallic nickel particles were detected on the grain surface for x = 0.2 and 0.3 using transmission electron microscopy. Temperature programmed reduction results indicate that the stable temperature for SFNM samples under reduction conditions decreases with Ni content. In addition, X-ray photoelectron spectroscopy analysis suggests that the incorporation of Ni affects the conductivity of SFNM through changing the ratios of Fe^{3+}/Fe^{2+} and Mo^{6+}/Mo^{5+}. $Sr_2Fe_{1.4}Ni_{0.1}Mo_{0.5}O_{6-\delta}$ shows the highest electrical conductivity of 20.6 $S·cm^{-1}$ at 800 ^oC in H_2. The performance of this anode was further tested with electrolyte-supported cells, giving 380 $mW·cm^{-2}$ at 750 ^oC in H_2, hence demonstrating that Ni doping in the B-site is beneficial for $Sr_2Fe_{1.5}Mo_{0.5}O_{6-\delta}$ anode performance.

1 Introduction

Solid Oxide Fuel Cells (SOFCs) have been regarded as ecocentric devices that convert chemical energy directly into chemical energy with high efficiency, low environmental pollution and good fuel flexibility.[1-2] Nickel/yttria-stablized zirconia (Ni/YSZ) is considered as the most common anode material for SOFCs, which exhibits excellent electrical performance with H_2 fuel, but is readily deactivated when operating on direct carbon fuels as nickel catalyzes the formation of carbon on the anode surface.[3-4] In order to overcome this problem, nickel-free alternative anodes with high conductivity and electrical catalytic activity have been investigated. Among these researches, mixed ionic-electronic conductor (MIEC) materials have attracted much attention owing to their excellent performance, such as high thermal chemistry stability and expanding triple phase boundary (TPB).[5-8]

Perovskite structure oxides are one of the most promising MIEC anode materials. The double perovskite anodes $Sr_2MgMoO_{6-\delta}$ (SMMO) are attractive due to their redox ability up to high temperature and direct use of natural gas as a fuel, whereas their low electrical conductivity represent a main constraint for this kind of material.[9-11] For the perovskite type oxides (ABO_3), researches have principally focused on the titanates and chromites, of these chromites demonstrate better performance than titanates.[12-13] The experimental results of Tao et al. indicated that the $La_{0.75}Sr_{0.25}Cr_{0.5}Mn_{0.5}O_3$ (LSCM) electrodes gave a performance comparable to that of Ni-based anodes. In terms of the electrical conductivity of LSCM anodes, it is difficult to achieve a value above 10 $S·cm^{-1}$ under reducing atmospheres. Moreover, its chemical stability and adhesion with electrolytes during operation are unsatisfactory. Despite this, studies of above materials have pioneered the use of perovskites as anodesinSOFCs.[14-16]

More recently $Sr_2Fe_{1.5}Mo_{0.5}O_{6-\delta}$ (SFM) has been reported as a very promising anode material with high electrical conductivity.[17]The as-reported material is chemically comparable with commonly used electrolytes like $Sm_{0.2}Ce_{0.8}O_{1.95}$ (SDC) and $La_{0.9}Sr_{0.1}Ga_{0.8}Mg_{0.2}O_3$ (LSGM). Among the SFM-based anodes, composite anodes have been used. For example SDC-SFM anodes were prepared to reduce polarization and, in addition, infiltrating SFM anode with a $Ni(NO_3)_2$ solution was shown to dramatically improve the anode performance.[18-19]For ABO_3 type oxides, substituting the transition metal at the B-site is also an effective approach to improve the performance. This approach can alter the cation valence and oxygen-vacancy concentration, which not only increases electronic conductivity but may also enhance the electrocatalytic oxidation activity.[20]However, few literatures have reported such B-site doping on the performance of SFM anodes.

In this work, Ni was introduced as a donor into the Fe-site of $Sr_2Fe_{1.5}Mo_{0.5}O_{6-\delta}$ system, instead of adding the NiO particles as a separate phase. Ni doping is anticipated to affect the transfer charge of Fe^{2+}/Mo^{6+} and to improve the electrical conductivity. The series of samples $Sr_2Fe_{1.5}Mo_{0.5}O_{6-\delta}$ (x = 0.05, 0.1, 0.2, 0.3, 0.4) referenced here as SFNMx, have been prepared in air. The chemical stability of SFNM samples in H_2 was measured by temperature programmed reduction. Moreover, the influence of both Ni-doping and Ni ex-solution under reducing conditions on SFM anodes is discussed, including crystal structure, element valence, conductivity and electrochemical impedance. Finally, the SFNM anodes electrochemical performance was further evaluated by fabricating the LSGM electrolyte-supported single cell.

2 Experimental sections

Perovskite SFNM materials were prepared using the combustion method.[21] Stoichiometric amounts of $Sr(NO_3)_2$, $Fe(NO_3)_3·9H_2O$, $Ni(NO_3)_3·6H_2O$ and $(NH_4)_6Mo_7O_{24}·4H_2O$ were used as the starting-materials. Citric acid was added to adjust the pH of the solution and glycine was used to promote the combustion. The resultant ash was calcined at 950 ^{o}C for 5 h in air to obtain pure the SFNM powders.

As the anode of SOFC, the properties of SFNM samples in reducing atmosphere were explored. The SFNM powders were first reduced under a continuous 3vol% H_2O humidified hydrogen gas flow at the rate of 50 mL·min^{-1} at 750 ^{o}C for 24 h. The phase purity and crystallinity of the as-calcined SFNM samples before and after reduction was examined by X-ray diffraction (XRD) (X' Pert PRO MPD) using Cu Kα radiation. In order to study the evolution of the surface element valence, X-ray photoelectron spectra (XPS) of both calcined and reduced samples was obtained using a MULT1LAB2000VG photoelectron spectrometer. The microstructure of the samples was monitored by means of scanning electron microscopy(SEM, FEI QUANTA-250) and transmission electron microscopy(TEM, FEI TECNAI F20).

Temperature programmed reduction (TPR) experiments were performed on a micromeritics apparatus (Chembet Pulsar TPR/TPD). This aims to measure the influence of Ni doping on the catalytic activity of SFNM anodes. The samples (30-50 mg) were loaded in the TPR quartz U-tube under Ar flow for 30 min and then were subjected to 10% H_2–90% Ar gas mixture (120 mL·min^{-1}) with a heating rate of 10 ^{o}C·min^{-1} up to 820 ^{o}C. The H_2 consumption results were recorded by a TCD for the subsequent analysis.

The electrical conductivity of SFNM was measured in 3vol% H_2O humidified hydrogen by a four-probe DC instrument (Keithley 2400, USA) with SFNM bars, which were prepared by pressing the SFNM powder into rectangular bars and sintering at 1200 ^{o}C for 5 h. Symmetrical cells with LSGM as electrolytes were measured by electrochemical impedance spectroscopy(PARSTAT 2273, USA) for SFNM anodes using a 10 mV DC signal in the frequency of 10 mHz to 100 kHz.

Single cells SFNM|LSGM|$Sr_2Fe_{1.4}Ni_{0.1}Mo_{0.5}O_{6-\delta}$ (SFN$_{0.1}$M) were fabricated in this work to study the performance of SFNM anodes. SFNM0.1 was selected as the cathode due to its excellent electrochemical performance as investigated in our previous work.[22] The LSGM electrolyte support (15 mm in diameter) was formed by dry-pressing LSGM powder (Fuel Cell, USA) uniaxially under 200 MPa and then sintered at 1450 ^{o}C for 8 h in air. The electrolyte was approximately 310 μm in thickness. Both the cathode and anode were applied to the electrolyte surface by screen-printing and co-fired at 1100 ^{o}C for 2 h. The obtained anode and the cathode were ca.37 μm and 21 μm, respectively. Ag paste was brushed on the cathode side as a current collector. The single cells were tested using an Arbin Instruments tester (Fuel Cell Test System, FCTS). The flow rate of the fuel gas(3vol% H_2O humidified hydrogen) was 50 mL min^{-1} and ambient air was used as the oxidant.

3 Results and discussion

3.1 Structural characterization.

XRD patterns of SFNM samples sintered at 950 ^{o}C for 5 h are shown in Fig.1a. The SFNM oxides crystallized in a single-phase perovskite structure with cubic symmetry and no impurity phases were observed. It is clear from Fig.1b that when the Ni content reaches 0.5, minor amounts of secondary phases are formed at ca.37°, 43° and 63°, which are attributed to NiO.[23] This result is in accordance with the report that the solubility limit of nickel into the chromites lattice is around 13% to 18% in the B-site and any excess nickel exists in the form of NiO.[24] Similarly with the perovskite structure, there is a solubility limit of nickel into the SFM and the value is ~20% based on the XRD results.

The SFNM0.1 sample were first reduced under 3vol% H_2O humidified hydrogen at 800 ^{o}C for 3 h, and XRD results show that the secondary phase $Sr_3FeMoO_{6.5}$ is formed (Figure.S1). After further reduction at 800 ^{o}C for 24 h, the $Sr_3FeMoO_{6.5}$ phase appears instead of the initial perovskite phase (Figure.S2). To identify the stable temperature of SFNM samples, the as-prepared powders were reduced at 750 ^{o}C for 24 h. The perovskite peaks are still maintained for x = 0.05, 0.1 shown in Fig.1c. While for the higher nickel content, the NiO impurity phase was detected (x =0.2, 0.3) indeed the main phase even splits for x = 0.4 as shown in Fig.1d. These peaks are assigned to $Sr_3FeMoO_{6.5}$. From the XRD results it can be concluded that lower nickel content SFNM materials are chemically stable under these reduction conditions. Even though the NiO phase appears in the SFNM0.2 and SFNM0.3 XRD pattern, it does not severely affect the performance of this material as an anode due to the integrity of the main phases. The $Sr_3FeMoO_{6.5}$ phase diffraction peaks are present upon reduction for SFNM0.4, which indicates the deterioration and limitation for SFNM0.4 as a SOFC electrode.
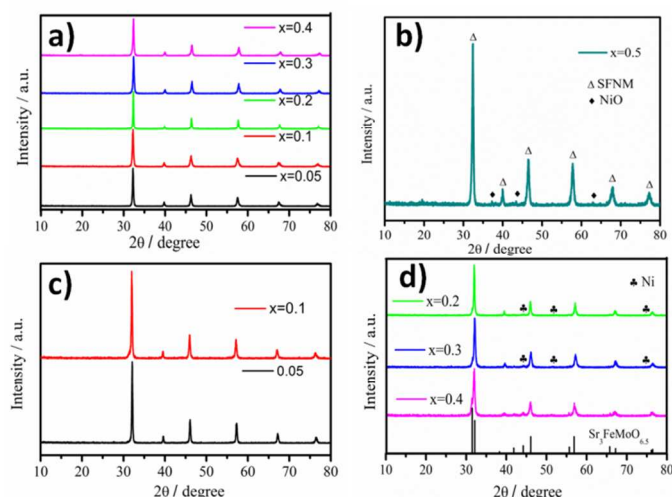
Fig.1 XRD patterns of SFNM powders after calcination at 950 °C in air for 5 h(a) x = 0.05-0.4, (b) x = 0.5; after reduction in H_2 at 750 °C for 24 h (c) x = 0.05-0.1, (d) x = 0.2-0.4

3.2 Temperature programmed reduction (TPR) analysis

TPR profiles of SFNM in a 10% H_2–90% Ar gas mixture are depicted in Fig.2, where the hydrogen consumption is measured as a function of the operating temperature. SFNM oxides present two reduction peaks at ~410 °C and ~500 °C, which are related to the reduction of Fe^{3+} and Mo^{6+}, respectively.[25-26] The nickel doping promotes the reduction of Fe^{3+} for x=0.05 and x=0.1. As the reduction peak shifts toward lower temperature compared to other ratios this suggests an improvement in the catalytic activity of SFNMs. As mentioned in section 3.1, the XRD patterns present the NiO phase for the reduced SFNM0.2, SFNM0.3 and SFNM0.4 materials, which is also supported by the TPR results. The weak peak at ~320 °C originates from the NiO released from the unstable reduced SFNM sample.[27] In addition, the main reason for unstable samples could be inferred
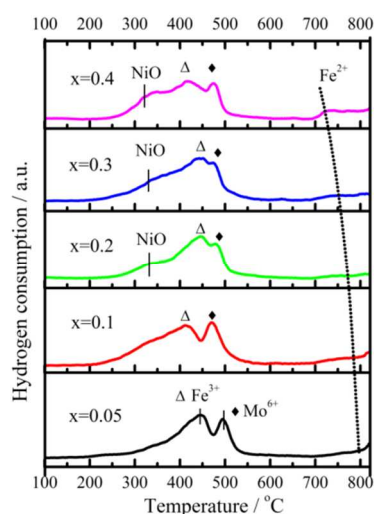
from the peaks appearing at 730 °C ~ 800 °C, which are ascribed to the reduction of Fe^{2+} in the perovskitebulk.[28] Once the cations in the bulk start to egress, the main phase peaks split, resulting in the instability. It is known from the TPR results that the unstable temperature for SFNM samples decreases from ~800 °C to ~725 °C with increasing Ni content (as the dashed line shows in Fig.2). This corresponds with the XRD analysis, hence SFNM samples (x = 0.05-0.3) are stable at 750 °C but not at 800 °C.

3.3 SEM and TEM analysis

As discussed previously, there are some minute changes in the SFNM crystal lattice after reduction, which could also be observed from the sample morphology by SEM and TEM. Different Ni content SFNM samples demonstrate similar morphology and Fig.3a shows the microstructure of the as-sintered SFNM0.1 oxide. After reduction under 3vol% H_2O humidified hydrogen, the microstructure of SFNM (x = 0.05 and 0.1) powders does not change visibly compared with the as-sintered samples. There are small reduced grains distributing uniformly on the surface when the nickel ratio exceeds 0.2 (Fig.3b). Corresponding to the SEM results, the changes are also confirmed by TEM. Taking the case of the SFNM0.1 sample, the prepared fresh samples have a smooth grain contour as shown in Fig.3c.After treatment under a reducing atmosphere, the morphology of SFNM (x = 0.05, 0.1) remains, but for higher Ni-containing samples (x = 0.2, 0.3, 0.4) the grain edge is altered with small particles appearing(Fig.3d). Moreover, XRD result showed that the re-oxidized SFNM0.2 sample did not present the NiO phase (Fig.S3).

3.4 X-ray photoelectron spectroscopy analysis

For perovskite oxides, the electrical performance is closely related to the presence of a mixed valence on the B-site.[29]As

Fig.2 H_2-TPR signals for the different SFM (x=0.05-0.4) samples: (Δ)Fe^{3+} ;(♦) Mo^{6+}; (------) Fe^{2+}
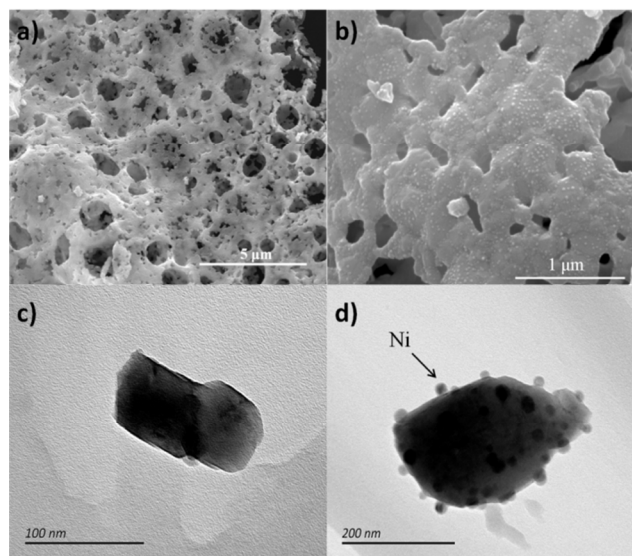

Fig. 3 SEM and TEM images of the as-prepared anode powders SFNM0.1 (a. c), and reduced samples SFNM0.2 (b. d).

different ratios of nickel are doped into the lattice, the rate of Fe^{2+}/Fe^{3+} and Mo^{5+}/Mo^{6+} couples changes distinctly. The X-ray photoelectron spectroscopy (XPS) was carried out here to study the elemental chemical states for SFNM materials.

Before the XPS analysis, SFNM samples were first treated at 750 °C and then cooled down to 80 °C under aH_2atmosphere.Fig.4 shows the Ni 2p, Fe 2p and Mo 3d spectra
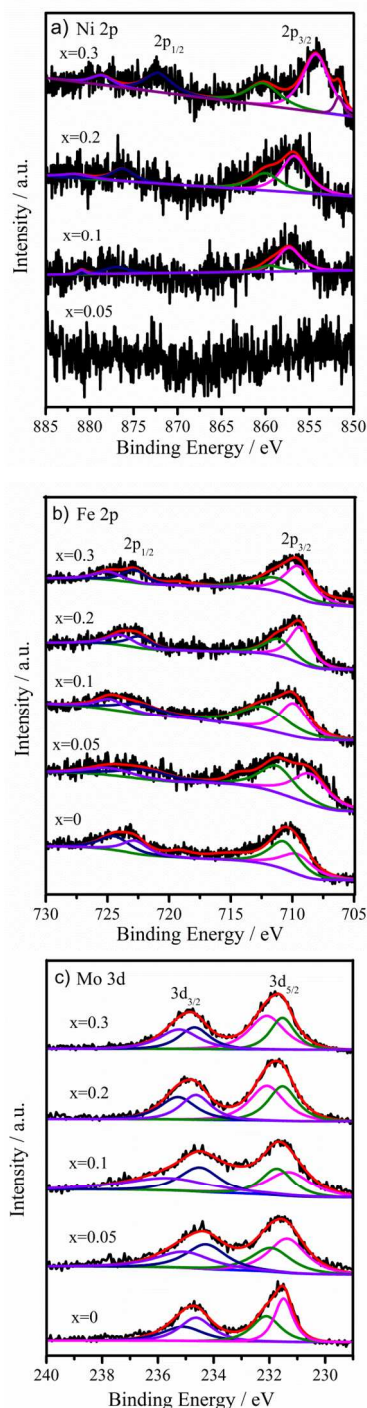

Fig.4 XPS spectra for the SFNM materials (x=0-0.3) for the Ni 2p (a), Fe 2p (b) and Mo 3d(c).

Table 1

Ratio of Fe 2p and Mo 3d peaks of SFNM obtained by X-ray photoelectron spectra

Sample	Fe^{2+}/Fe^{3+} ratio	Mo^{6+}/Mo^{5+} ratio
X=0	1.22	1.11
X=0.05	1.10	1.01
X=0.1	0.97	0.94
X=0.2	1.42	1.14
X=0.3	1.56	1.35

taken at room temperature using the reduced samples. For Ni 2p of SFNM0.1 (Fig.4a), the peaks of binding energy at 856 eV and 877 eV are assigned to Ni $2p_{3/2}$ and Ni $2p_{1/2}$, there are also satellite peaks appearing at ~6 eV from the main $2p_{3/2}$ and $2p_{1/2}$line.[30]The Ni in SFNM oxides (x = 0.05-0.2) all present a divalent valence state (Ni^{2+}) without other valences. Among the results, it is worth noting that one peak appears at 852 eV for the SFNM0.3, which is related to metallic nickel (Ni^0).[31]As calculated from the fitting results of Ni^{2+}/Ni^0 most of the nickel is still in the lattice with only a fraction being reduced to metallic nickel. The Ni^{2+} peak for SFNM0.05andNi^0peak for SFNM 0.2 are not obvious.

Data analysis of the Fe 2p binding energy in SFNM is depicted in Fig.4b. For all samples, iron exists in mixed states with Fe^{2+} and Fe^{3+}. It is reported that the peaks of binding energy of $Fe^{2+}2p_{3/2}$ and $Fe^{2+}2p_{1/2}$ are located at 709.0 eV and 722.6 eV, and for Fe^{3+} the two locations are at 711.0 eV and 724.6 eV, respectively.[32]Fig.4b also reveals that the binding energy of Fe $2p_{3/2}$ decreases with Ni content, which indicates that the proportion of Fe^{2+}/Fe^{3+} is changed by Ni doping. By fitting and computation, the ratio of Fe^{2+}/Fe^{3+}increases at first and then declines along with the Ni content as shown in Table.1.

The Mo 3d core level spectra of SFNM (x = 0-0.3) samples are shown in Fig. 4c, which display two broad peaks on the binding energy scale. By curve fitting the Mo excitations give rise to four peaks that are attributed to Mo^{6+}(232.1 eV and 235.3 eV) and Mo^{5+} (231.3 eV and 234.5 eV).[33] As can be seen from the figure, with increasing Ni the binding energy of Mo $3d_{5/2}$ increases while that of Mo $3d_{3/2}$ decreases. Moreover, the ratio of$Mo^{6+}/$ Mo^{5+}presents the same trend as theFe^{2+}/Fe^{3+} couple.

The above detailed XPS analysis clearly suggests that the mixed valence state couples Fe^{2+}/Fe^{3+} and Mo^{6+}/Mo^{5+} exist in SFNM materials, and no parasitic phases are detected in terms of Fe^0 and Mo^{4+}. A small amount of Ni^0 appears when x = 0.3, which corresponds to the XRD and TPR results. Even though XPS measurement is used to study the surface of materials, we consider that the elements are distributed uniformly in the sample. Furthermore, the presence of Ni changes the proportion of other two ion pairs. The ratio of Fe^{2+}/Fe^{3+} decreases from 1.22(x = 0) to 0.97 (x = 1) and then upward to 1.56 (x = 0.3).Similarly, the value of Mo^{6+}/Mo^{5+} first goes down to 0.94 (x = 1) from 1.11(x = 0) and up to 1.35(x=0.3). The introduction of Ni has an impact on the reaction equilibrium, $Fe^{2+}+ Mo^{6+}↔Fe^{3+}+Mo^{5+}$. The difference value between the

total $Fe^{2+}+Mo^{6+}$and $Fe^{3+}+Mo^{5+}$ becomes the least when x = 0.1. Therefore the reaction equilibrium appears to be easier toward the two sides in the process of reduction/oxidation reaction. Accordingly, the substitution of Ni into the B-site of SFM lattice is anticipated to affect the electrochemical properties of SFNM materials.

3.5 Electrical characteristics of SFNM

3.5.1 CONDUCTIVITY

Fig.5 shows the electricity conductivity (σ) of SFNM (x = 0-0.3)samples versus temperature in 3vol% H_2O humidified hydrogen. The ionic conductivity is negligible compared with the electronic conductivity for SFM materials.[17]Therefore, the measured total conductivity is primarily related to the electronic conductivity. As the SFNM samples were not stable at 800 ^{o}C after long reduction times, the measurement was operated during the heating process after stability at each testing temperature. Overall, the σ value is appropriately linear with temperature for x = 0.05-0.2 and is higher than that of SFM. At 800 ^{o}C, the σ value reaches the maximum when x = 0.1, that is 20.6S·cm^{-1}, which is suitable for anode materials. With an increase of reduction time, the σ value decreases sharply because theSr$_3$FeMoO$_{6.5}$phase appears (as mentioned in section 3.1), indicating that theSr$_3$FeMoO$_{6.5}$phasedoes not contribute to the high electronic conductivity of SFNM. In SFM, the electrical conductivity is derived from the exclusive movement of electrons or electron holes through the Fe-O-Fe path. The introduction of the transition metal Ni is expected to enhance the strong hybridization between p states of oxygen and d states of iron, so that the reduced SFNM delocalize the extra charge to retain metallic character.[34]Additionally, the predominant electronic configuration changes from Fe^{2+}/Mo^{6+} to $Fe^{3+}/Mo^{5+}$when the Ni content reaches 0.1, resulting in the increase of electronic conductivity. With Ni content further increasing, the ratio of Fe^{2+}/Mo^{6+} gradually goes back to, or exceeds, the original level and the σ value diminishes simultaneously. This indicates that theFe^{3+}/Mo^{5+} ion pair contributes to the electronic conductivity, which agrees with the report by Zhang et.al[33] The unit cell of SFNM shrinks with further increasing the Ni content, which may have brought the conduction orbits closer between Fe and Mo, and possibly restrained the conduction of the electrons resulting in the
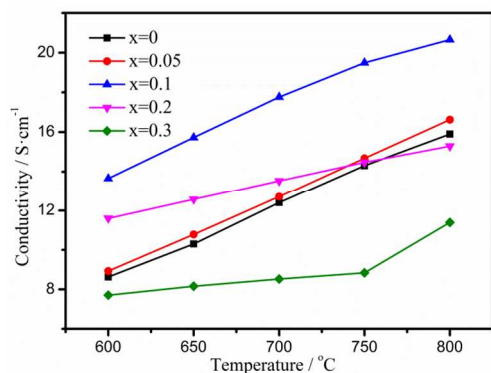
conductivity decrease with Ni from 0.1 to 0.3.[22] Due to the egression of Ni from the lattice, the effect of weakening the Fe-O bonds has shrunk hence resulting in the drop of electrical conductivity.

3.5.2 IMPEDANCE SPECTRA TEST

Based on measurement data, SFNM0.1 demonstrates the highest electricity conductivity. In order to further understand this result, typical impedance spectra of SFNM anodes were measured using a symmetric cell configuration in hydrogen as shown in Fig.6.As can be seen in Fig.6a, the electrode polarization resistance (R_p) values of the samples are significantly affected by different Ni doping concentrations in the temperature range of 650-800 ^{o}C. The R_p values gradually decrease with increasing nickel doping from x = 0 to 0.1 and then increase with Ni addition. The minimum R_p is 0.65 Ω·cm^2, obtained at 800 ^{o}C when x =0.1.Furthermore, SFNM(x = 0.05-0.2) shows a smaller polarization resistances when compared with SFM samples, which means that the electrode performance is improved by Ni doping. In contrast, a higher content of Ni (x = 0.3) results in an increase of the R_p value. This might be caused by the fact that the SFNM0.3 is not chemical stable during the test given the large excess of Ni. Consequently, the crystal structure change degrades the SFNM anode performance. Fig. 6b shows the impedance spectra at 750 ^{o}C for the SFNM anodes with various Ni contents. The R_p
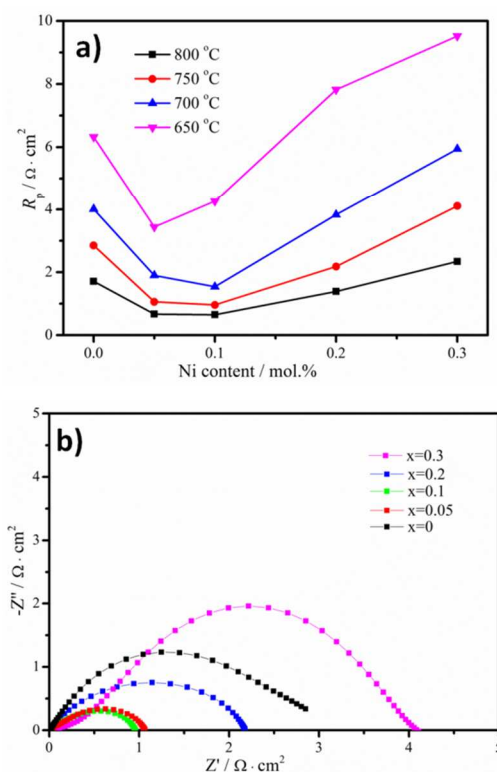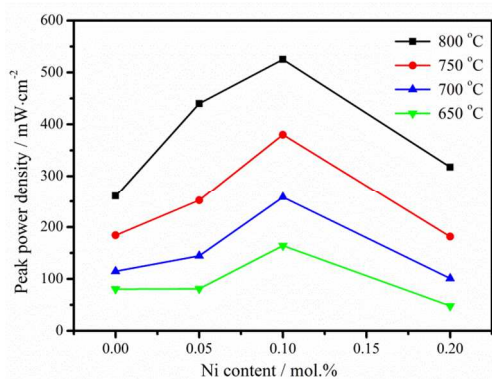
Fig.7 Peak power density of single cells with SFNM|LSGM|SFN$_{0.1}$M configuration as a function of Ni content in SFM anode

Fig.8 Performance of SFNM0.1|LSGM|SFN0.1M cell with H$_2$ as fuel. (a) I–V and I–P curves; (b) impedance spectra of single cell under open circuit conditions;(c)the stability test at 750 °C.(d) cross-section image of single cell after testing.

values are 2.85, 1.06, 0.96, 2.18and 4.11 $\Omega \cdot cm^2$ for x = 0, 0.05, 0.1, 0.2, 0.3, respectively. The results obtained here are in agreement with the above measurement.

3.5.3 ELECTRICAL PERFORMANCE OF SINGLE CELLS

The effect of Ni substitution on SFNM(x = 0-0.2) anodes was further investigated with single cells fabricated with a LSGM electrolyte and SFN$_{0.1}$M cathode. Fig.7 displays the peak power density of the as-prepared different Ni content cells tested at various temperatures with H$_2$ as fuel. The maximum power density was achieved with 0.1 mol. % Ni doped at 800 °C, whichis530 mW·cm^{-2}. The results are generally consistent with the EIS and conductivity analysis and confirms that appropriate Ni doping (x = 0.05-0.2) is beneficial for the improvement of electrode performance. The cell performance is expected to further improve if thinner electrolytes and composite anodes are employed.

Fig.8a shows the I–V and I–P curves with SFNM0.1|LSGM|SFN$_{0.1}$M configuration cells operating at 650–800°C. The cells demonstrate maximum power densities of 530, 380, 258 and 164 mW·cm^{-2}at 800, 750, 700 and650 °C with H$_2$ as fuel, respectively. The corresponding measured cell impedance spectra are shown in Fig. 8b. The high-frequency intercept on the real axis represents the ohmic resistance (R_Ω) and the distance between the two intercepts on the real axis represents the polarization resistance (R_p). It can be seen that the values of R_p and R_Ω decrease with increasing temperature. The values of R_p are 0.62, 0.31, 0.11$\Omega \cdot cm^2$ at 700, 750, 800 °C, respectively. The total resistance is mainly controlled by R_p and reducing R_p is crucial to optimize the cell performance. As shown in Fig. 8c, the SFNM0.1|LSGM|SFN$_{0.1}$Msingle cell showed stable performance for 15 h with no obvious degradation under a constant current density of 0.75A cm^{-2} at750°C. From the cross-section image of single cell after testing (Fig. 8d), it can be observed that there is no separation between SFNM anode and LSGM electrolyte. All these results suggest the excellent electrochemical performance of SFNM anode, indicating that SFNM is a promising candidate as the anode for IT-SOFCs.
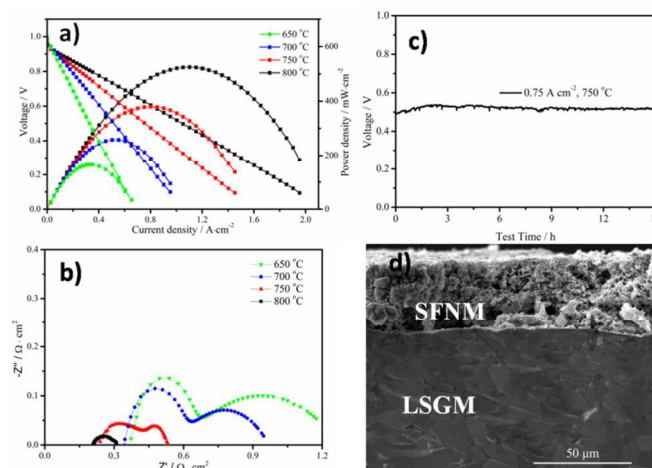
4 Conclusions

Sr$_2$Fe$_{1.5-x}$Ni$_x$Mo$_{0.5}$O$_{6-\delta}$(x = 0.05, 0.1, 0.2, 0.3, 0.4) samples have been investigated as anode materials. The XRD analysis indicate that the perovskite structure is maintained for SFNM(x = 0.05-0.1) oxides and NiO egresses from the bulk lattice (x = 0.2, 0.3, 0.4) under reducing atmosphere. The TPR experimental results further confirm that the peaks located at ∼ 300 °C are related to metallic nickel for SFNM0.3 and SFNM0.4 samples. The unstable temperature for SFNM samples decreases from ∼800 °C to ∼725 °C with increasing Ni content. Moreover, the ratios of Fe^{2+}/Fe^{3+} and Mo^{6+}/Mo^{5+}have been changed owing to the Ni doping as demonstrated by XPS analysis. The ion pair Fe^{3+}/Mo^{5+} achieves the maximum value when x = 0.1, which benefits electron transfer between two ion pairs and improves the reduction/oxidization reaction rate. Additionally, the introduction of Ni enhances the strong hybridization of Fe d−O p so as to retain a metallic character. Consequently electrical characterizations show that SFNM0.1 demonstrates the lowest R_p and highest conductivity value when compared with other Ni contents. The maximum power densities of a single cell fabricated with theSFNM0.1 anode are 530 and 380W·cm^{-2} at 800 and 750 °C, respectively. These results indicate that doped Ni enhances the performance of SFM materials as anodes.

Acknowledgements

Notes and references

[a] Beijing Key Laboratory for Chemical Power Source and Green Catalysis, School of Chemical Engineering and Environment, Beijing Institute of

Journal of Materials Chemistry A Accepted Manuscript

Technology, Beijing, 100081, China, E-mail: qjinshuo@bit.edu.cn; bitkeningsun@163.com; Tel&Fax:0086-10-68918696

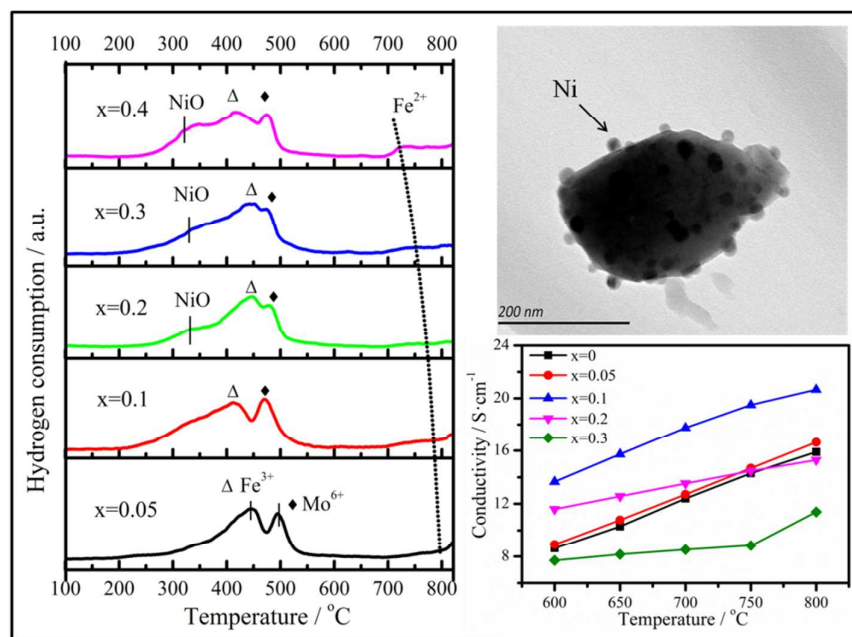*b School of Chemistry and Chemical Engineering, Queen's University Belfast, Belfast, Northern Ireland BT9 5AG, United Kingdom*

1   Z. L. Zhan and S. A. Barnett, *Science*, 2005, **308**, 844-847.
2   R. M. Ormerod, *Chem. Soc. Rev.*, 2003, **32**, 17-28.
3   A. Atkinson, S. A. Barnett, R. J. Gorte, J. T. S. Irvine, A. J. McEvoy, M. Mogensen, S. C. Singhal and J. Vohs, *Nat Mater.* 2004, **3**, 17-27.
4   L. Yang, S. Z. Wang, K. Blinn, M. F. Liu, Z. Liu, Z. Cheng and M. L. Liu, *Science*, 2009, **326**, 126-129.
5   Z. X. Xie, H. L. Zhao, T. Chen, X. Zhou and Z. H. Du, *Int. J. Hydrogen Energy*,2011, **36**, 7257-7264.
6   J. B. Goodenough and Y.H. Huang, *J. Power Sources*, 2007, **173**, 1-10.
7   H. Kan and H. Lee, *Catal. Commun.*, 2010, **12**, 36-39.
8   S. Zha, Z. Cheng and M. Liu, *Electrochem. Solid-State Lett.*, 2005, **8**, A406-A408.
9   Y.H. Huang, R. I. Dass, Z.L. Xing and J. B. Goodenough, *Science*, 2006, **312**, 254-257.
10 S. Vasala, M. Lehtimäki, Y. H. Huang, H. Yamauchi, J. B. Goodenough and M. Karppinen, *J. Solid State Chem.*, 2010, **183**, 1007-1012.
11 D. Marrero-López, J. Pena-Martinez, J. C. Ruiz-Morales, D. Pérez-Coll, M. A. G.Aranda and P. Nunez, *Mater. Res. Bull.*, 2008, **43**, 2441-2450.
12 H. Kurokawa, L. Yang, C. P. Jacobson, L. C. De Jonghe and S. J. Visco, *J. Power Sources*, 2007, **164**, 510-518.
13 S. P. Jiang and S. H. Chan, *J. Mater. Sci.*, 2004, **39**, 4405-4439.
14 S. W. Tao and J. T. S. Irvine, *J. Electrochem. Soc*, 2004, **151**, A252-A259.
15 J. Wan, J. H. Zhu and J. B. Goodenough, *Solid State Ionics*, 2006, **177**, 1211-1217.
16 Y.H. Huang, R. I. Dass, J. C. Denyszyn and J. B. Goodenough,*J. Electrochem. Soc.*, 2006, **153**, A1266-A1272.
17 Q. Liu, X. H. Dong, G. L. Xiao, F. Zhao and F. L. Chen, *Adv. Mater.*, 2010, **22**, 5478-5482.
18 B. B. He, L. Zhao, S. X. Song, T. Liu, F. L. Chen and C. R. Xia, *J. Electrochem. Soc.*, 2012, **159**, B619-B626.
19 G. L. Xiao and F. L. Chen, *Electrochem. Commun.*, 2011, **13**, 57-59.
20 S. Cho, D. E. Fowler, E. C. Miller, J. S. Cronin, K. R. Poeppelmeier and S. A. Barnett, Energ EnvironSci, 2013, 6, 1850-1857.
21 N. N. Dai, Z. L. Lou, Z. H. Wang, X. X. Liu, Y. M. Yan, J. S. Qiao, T. Z. Jiang and K. N. Sun, *J. Power Sources*, 2013, **243**, 766-772.
22 N. N. Dai, J. Feng, Z. H. Wang, T. Z. Jiang, W. Sun, J. S. Qiao and K. N. Sun, *J. Mater. Chem. A*, 2013, **1**, 14147-14153.
23 A. Akbari-Fakhrabadi, R. E. Avila, H. E. Carrasco, S. Ananthakumar and R. Mangalaraja, *J. Alloys Compd.*, 2012, **541**, 1-5.
24 W. Kobsiriphat, B. D. Madsen, Y. Wang, M. Shah, L. D. Marks and S. A. Barnett, *J. Electrochem. Soc.*, 2010, **157**, B279-B284.
25 P. Salerno, S. Mendioroz and A. LópezAgudo, *Appl. Clay Sci.*, 2003, **23**, 287-297.
26 G. L. Xiao, C. Jin, Q. Liu, A. Heyden and F. L. Chen, *J. Power Sources*, 2012, **201**, 43-48.
27 T. Klimova, M. Calderón and J. Ramírez, *Appl. Catal. A*, 2003, **240**, 29-40.
28 G. L. Xiao, Q. Liu, S. W. Wang, V. G. Komvokis, M. D. Amiridis, A. Heyden, S. G. Ma and F. L. Chen, *J. Power Sources*, 2012, **202**, 63-69.
29 H. X. Gu, Y. Zheng, R. Ran, Z.P. Shao, W. Q. Jin, N. P. Xu and J. Ahn, *J. Power Sources*, 2008, **183**, 471-478.
30 M. Lo Faro, M. Minutoli, G. Monforte, V. Antonucci and A. S. Aricò, *Biomass Bioenergy*, 2011, **35**, 1075-1084.
31 M. C. Biesinger, B. P. Payne, A. P. Grosvenor, L. W. Lau, A. R. Gerson and R. S. C. Smart, *Appl. Surf. Sci.*, 2011, **257**, 2717-2730.
32 T. Yamashita and P. Hayes, *Appl. Surf. Sci.*, 2008, **254**, 2441-2449.
33 L. L. Zhang, Q. J. Zhou, Q. He and T. He, *J. Power Sources*, 2010, **195**, 6356-6366.
34 A. B. Muñoz-García, D. E. Bugaris, M. Pavone, J. P. Hodges, A. Huq, F. L. Chen, H.C. zurLoye and E. A. Carter, *J. Am. Chem. Soc.*, 2012, **134**, 6826-6833.

Journal of Materials Chemistry A Accepted Manuscript

The unstable temperature for $Sr_2Fe_{1.5-x}Ni_xMo_{0.5}O_{6-\delta}$ materials in H_2 decreases with the increment of Ni content. Egressed Ni particles were detected for samples with higher Ni content (x>0.1). $Sr_2Fe_{1.4}Ni_{0.1}Mo_{0.5}O_{6-\delta}$ shows the highest electronic conductivity of 20.6 S·cm^{-1} at 800 ^{o}C.